

https://dspace.org/

Characterization Kinetics and thermodynamic evaluation of struvite produced using ferrochrome slag as a magnesium source

Langa Moyo; Geoffrey Simate; N Hobane; C Dube

https://hdl.handle.net/10539/41937
SCOPUS

Downloaded from a DSpace repository. https://dspace.org/

South African Journal of Chemical Engineering 47 (2024) 83–90

Contents lists available at ScienceDirect

South African Journal of Chemical Engineering

journal homepage: www.elsevier.com/locate/sajce

Characterization, kinetics and thermodynamic evaluation of struvite produced using ferrochrome slag as a magnesium source

L.B Moyo [a,b,*], G.S. Simate [a], N Hobane [b], C Dube [b]

[a] School of Chemical and Metallurgical Engineering, University of the Witwatersrand, Private Bag 3, Wits, 2050, Johannesburg, South Africa
[b] Department of Chemical Engineering, National University of Science and Technology, Box AC 939 Ascot, Bulawayo, Zimbabwe

ARTICLE INFO

Keywords:
Crystallization
Struvite
Kinetics
Thermal analysis
Activation energy
Ferrochrome slag

ABSTRACT

There is limited data on studies that have focused on the kinetics, thermodynamics, and characterization of struvite crystallization from alternative magnesium sources. This study focused on thermal analysis of struvite (produced using ferrochrome slag as a magnesium source) and the results indicated that the residual quantities of struvite were lower than the theoretical mass loss of struvite of 51.42%. When using ferrochrome slag (FCS) as the magnesium source, 47.9%, 47.4%, and 46.9% losses in mass were observed for heating rates of 5°C/min; 10°C/min and 15°C/min respectively. The mean activation energies for struvite produced using FCS were deduced using isoconversional kinetic methods and ranged from 49.81to 56.20 kJ/mol which is very similar to the activation energies deduced using $MgCl_2$. The study also focused on the surface morphology, and particle size of the final product at different pH and N:P ratios. The final particle size distribution of the product was significantly influenced by the solution pH. To improve the crystal growth kinetics for both $MgCl_2$ and FCS, a high ratio of N:P molar ratios should be adopted. The product's highest median particle size was obtained using FCS as the magnesium source at a low pH. Median particle size increased with decrease in pH, at a pH of 7.5 the recorded median particle size was 96 μm whilst, the lowest was 31 μm at a pH of 9.5. The highest percent of fines (<10 μm) was recorded at a pH of 9.5 using FCS as magnesium source in the metastable region of struvite precipitation whereas at a pH of 7.5 no fines (<10 μm) were recorded. SEM images confirmed that the struvite underwent morphological changes when prepared with FCS in comparison to that produced using $MgCl_2$. The surface morphology of the finished product demonstrated the presence of irregular shaped particles, due to presence of impurities. The kinetic data showed that struvite precipitation was limited by the chemical reaction step. Model fitting was used to determine the reaction control mechanism and the average activation energies obtained by four model free methods were FWO (56.2), KAS (51.67) Starink (49.61) and Tang (49.81) kJ/mol, indicating that the FWO method was the least accurate method. The thermodynamic data indicated that the thermal degradation of struvite crystals has a high degree of disorder, and the process is endothermic, irreversible, and non-spontaneous.

1. Introduction

The cost of fertilizers has increased almost threefold what it was before the Russia-Ukraine war. Around 25% of the nitrogen fertilizer used worldwide is produced in Russia (CNBC, 2022). Consequently, it is imperative to consider fertilizer sources other than the traditional mineral fertilizers as this has directly affected the food and agricultural sector in Africa. For example, Zimbabweans primarily depend on agriculture and most rural economic activities are aligned to agriculture, making agriculture the foundation of the country's economy. Approximately 60 to 70% of the population receives employment and income from agricultural operations, which also produce 60% of the raw materials needed by the industrial sector and 40% of all export revenues (Fao.org, 2022). Moreover, about 17% of Zimbabwe's GDP is derived from agriculture. In this regard, beneficiation of nutrients from animal wastewater to form struvite a slow-release fertilizer using readily available resources is attractive to economies such as that of Zimbabwe. Furthermore, the problems associated with the accumulation of struvite on the equipment surfaces of anaerobic digestion and post-digestion processes in the wastewater treatment industry have a commercial

* Corresponding author.
E-mail address: langabmoyo@gmail.com (L.B Moyo).

https://doi.org/10.1016/j.sajce.2023.10.012
Received 14 March 2023; Received in revised form 7 September 2023; Accepted 23 October 2023
Available online 24 October 2023
1026-9185/© 2023 The Authors. Published by Elsevier B.V. on behalf of South African Institution of Chemical Engineers. This is an open access article under the CC BY-NC-ND license (http://creativecommons.org/licenses/by-nc-nd/4.0/).

impact through major downtime, loss of hydraulic capacity, and increased pumping and maintenance costs (Moyo et al., 2023). Since struvite can be a concern in wastewater treatment facilities, the circumstances for its development found in wastewater treatment plants can be used to extract struvite. However, one of the major drawbacks of nutrient recovery is the high chemical costs required to precipitate the nutrients as struvite. The use of conventional magnesium sources such as magnesium chloride for precipitation of struvite accounts for up to 75% of the chemical costs (Moyo et al., 2023, 2022b). In this regard, it is imperative to find alternative cheap magnesium sources such as ferrochrome slag (FCS) for use in struvite crystallization (Moyo et al., 2022a; Shaddel et al., 2020).

The conventional process of ferrochrome making involves the carbothermic reduction of chromite ore where around 1.2–1.5 tons of slag containing 8–12% of chromium oxide is generated per ton of hot metal. FCS significantly comprises of 27–33% SiO_2, 15–25% Al_2O_3, 20–35% MgO and 10–15% iron chromium compounds (Das et al., 2023). A substantial amount of FCS is disposed through dumping, thus it becomes a burden to the environment. Various scholars have reported FCS as a hazardous waste due to the oxidation of Cr(III+) to Cr(VI+), present in FCS in an oxidizing environment (Das et al., 2023). The beneficiation of Mg from FCS has been demonstrated to be feasible through leaching with hydrochloric acid with recoveries of up to 88.2%, the leachate can be used for phosphorus recovery through struvite crystallization (L.B. Moyo et al., 2022).

A wide range of phosphorus recovery technologies have been established, including electrolysis, adsorption, biological phosphorus removal, chemical precipitation, and crystallization (Santiviago et al., 2022). Polyphosphate-accumulating organisms are used in biological phosphorus removal to store phosphorus in their cells. However, this approach is constrained by the scarcity of carbohydrate supplies and the challenge of cultivating pure bacteria (Zhang et al., 2017). On the other hand, the process of chemical precipitation may use expensive chemicals and generate significant amounts of chemical sludge. In contrast, electrolysis is constrained by its limited ability to handle waste water and by the need for frequent electrode replacement. Whereas, recovering phosphorus from waste water using chemical adsorbents is expensive so cheaper and more efficient adsorbents are necessary for research (Li et al., 2013). In contrast, in this case recovering phosphorus through crystallization by using a waste material such as FCS is envisaged to be a more practical and cost-effective method, provided that the crystallization conditions are optimal.

Nucleation and crystal growth are the two steps in the production of struvite crystals. It is difficult to predict or control these stages because they are influenced by a number of physico-chemical variables, including the pH of the solution from which struvite may precipitate, super saturation, mixing energy, temperature, and the presence of foreign ions (Song et al., 2021). These variables also include phenomena of matter transfer between solid and liquid phases and reaction kinetics. The aforementioned variables directly affect properties that include, particle size distribution, crystal shape, degree of agglomeration, caking behavior, and purity (Ping et al., 2016; Shaddel et al., 2020). It is imperative to optimize the properties as other functional elements of the end usage, such as filterability, flowability, and compaction behavior, are significantly influenced by these properties. In many crystallization methods, the flake shape and long needle shape crystals, for instance, are undesired (Burns et al., 2021).

A difficult non-linear natural occurrence, crystallization presents modeling and control challenges. Any solid phase that forms from an aqueous solution is also governed by kinetics and solution thermodynamics. As a result, each unique system requires specialized investigation to properly understand the factors that affect crystallization (Wu et al., 2022; Muryanto et al., 2014). Struvite crystallization kinetic and thermodynamic studies using alternative magnesium sources such as FCS has not received much attention. Therefore, in this study, using a model-fitting technique, kinetic studies were undertaken. This work uses thermogravimetric analysis, 4 non-isothermal methods and 15 different models to offer a thorough kinetic, activation energy and analysis of struvite crystallization. Struvite crystallization has been examined utilizing chemical reactions and diffusion, geometric, and nucleation models using the Coats-Redfern, a non-isothermal model-fitting integral technique. Moreover, in investigating the thermodynamic aspects of struvite crystallization estimation of the activity coefficients and the enthalpy of struvite formation are derived from experimental data and compared with literature to ascertain that the compound formed is struvite. The study is imperative as the knowledge regarding the kinetics and thermodynamics that are involved in struvite crystallization is fundamental in determining the optimal conditions for an efficient crystallization process.

2. Materials and methods

2.1. Materials

The filtrate from the anaerobic digestate of pig waste was put into 2 L containers. The pH was adjusted to between 7.5 −9.5, which is the desired alkaline conditions, using 5 M NaOH (Moyo et al., 2022a). Sodium dihydrogen phosphate was used to modify the molar ratio of N:P. FCS was leached using 5 M HCl (Shaddel et al., 2020), this was used as the Mg source to adjust the Mg:PO_4 ratio. The struvite precipitation was undertaken at room temperature, mixing took place in an orbital shaker for one hour at 200 rpm. The precipitate, was centrifuged at 3000 rpm for 10 min, cleaned with deionized water, and then dried in a drying oven at 40 °C for 24 h (Moyo et al., 2023).

2.2. TGA analysis

Struvite thermal properties were measured using TGA. A 10 mg sample of struvite was tested using a thermo-gravimetric analyzer (Q 500 series, TA Instruments, USA). To investigate the struvite mass-loss from 50 to 350°C, three different heating rates of 5°C/min;10°C/min and 15°C/min were investigated. An inert atmosphere was kept at a rate of 60 ml/min using nitrogen as a carrier gas. The experiments were conducted in duplicate to achieve the lowest error and best accuracy. The information from the TGA was useful in estimating the kinetics of disintegration of the struvite.

2.3. Particle size

Malvern Mastersizer (3000TM, UK) was used to analyze the particle size. The particle size distribution of a sample is provided using this apparatus, which makes use of the laser diffraction technique. This technique for analyzing particle size is used for sizes between 0.1 μm and 3. 5 mm. The suitable size range can only be increased above 3.5 mm and below 0.1 μm under extraordinary circumstances. In a laser diffraction test, a laser beam travels through a sample of suspended particles. Depending on the particle size, these particles diffract or scatter light at a specific angle. In comparison to the laser beam, larger particles diffract light at smaller angles, whereas smaller particles diffract light at larger angles. Data collection and analysis enabled the total particle size distribution to be determined.

2.4. Surface morphology

Scanning electron microscopy (SEM) was used to examine the struvite's surface morphology. The SEM ZEISS SIGMA 300VP system was used to do the analysis. An accelerating voltage of 20 kV and a dimension measuring 20 or 100 μm were used to analyze the struvite crystals.

2.5. Kinetics and thermodynamic analysis

By fitting the experimental data captured under dynamic heating

circumstances, the model fitting approaches for kinetic analysis for thermal degradation are examined. Mathematical functions called kinetic models are created using specific physico-geometrical assumptions about the structure of the reactants and the reaction driving force. In this study, the Coats-Redfern method, one of the most used models, and four model-free procedures were utilized and compared. These methods were adopted due to their simplicity. TGA was used to calculate the weight variations of struvite produced using $MgCl_2$ and FCS samples as a function of temperature to analyze the kinetics of struvite thermal degradation and determine the activation energy. These dynamics can be studied using either isothermal or non-isothermal techniques. The second approach is thought to be simpler because it requires fewer experiments and does not account for changes in the chemical and physical properties of the sample. Based on TGA data, kinetic parameters are calculated using model-free or model-based approaches. The model-free approach has the advantage that the reaction mechanism can be identified without needing to compute the activation energy.

The TGA results can be illustrated as a function of fraction conversion shown by equation 1;

$$\alpha = \frac{m_o - m_t}{m_o - m_f} \tag{1}$$

Where, m_o and $m_f$represent the initial and final sample weight; m_t refers to the instantaneous mass of sample.

The activation energies of the struvite produced with FCS were determined in this investigation using four widely used isoconversional kinetic methods. Their corresponding linear equations are shown as Eq. (2), (3), (4), and (5) (Polat and Sayan, 2020). The Flynn-Wall Ozawa method (FWO), The Kissinger-Akahira-Sunose (KAS) method, The Starink method, and Tang method respectively. These four models not only achieve consistent apparent activation energy (E), but they also avoid inaccuracies caused by different assumptions of reaction mechanism functions.

The Flynn-Wall Ozawa (FWO) model

$$\ln\beta = \frac{\ln AE}{Rg(x)} - \frac{E}{RT} \tag{2}$$

The Kissinger-Akahira-Sunose (KAS) model

$$\frac{\ln\beta}{T^2} = ln\frac{AR}{Eg(x)} - \frac{E}{RT} \tag{3}$$

The Starink model

$$\frac{\ln\beta}{T^{1.92}} = C - 1.008\frac{E}{RT} \tag{4}$$

The Tang model

$$\frac{\ln\beta}{T^{1.8947}} = C - 1.0015\frac{E}{RT} \tag{5}$$

where t is the induction time, which is the time interval for the thermal degradation process, T is the absolute temperature, β refers to the heating rate (dT/dt), g(α) is the integrated reaction model, and α is the conversion rate, A is the pre-exponential factor, E is the activation energy, R is the gas constant. The gradients of the lines from the plots of ln (β) vs 1/T, ln(β/T^2) versus 1/T, ln (β /$T^{1.92}$) versus 1/T, and ln(/$T^{1.8947}$) versus 1/T for the FWO, KAS, Starink, and Tang methods, respectively, can be used to estimate E for any given value. Fig 2(a) to (d) show the plots used to depict the activation energies.

The Pre exponential factor (A) was deduced from the Kissinger equation upon rearranging as shown by Eq. (6) (Polat and Sayan, 2020);

$$A = \frac{\beta E exp\left(E/RT_{peak}\right)}{RT_{peak}^2} \tag{6}$$

Erying equations were used to calculate the thermodynamic parameters of the struvite crystals including enthalpy change ΔH, Gibbs free energy change ΔG and entropy change ΔS (Guan et al., 2023)

The values of the thermodynamic which variables include the change in enthalpy, Gibbs free energy and entropy, are generally used to determine the feasibility, direction and energy variations in the thermal conversion process, can be calculated using equations (7), (8), (9). Enthalpy denotes the energy difference between the involved reactants and the formed products. The relevant thermal degradation process is endothermic if the values are positive. The disparity between and E values also shows the potential energy barrier for the thermal conversion process over time. The analogous reaction may be thought to be advantageous for the production of an activated complex if the difference between and E is smaller than 7 kJ/mol. This is used to reflect the reaction difficulty and reaction direction and indicates the gross energy increase of the reaction system during the thermal conversion process. Larger values imply a reduced likelihood of the associated thermal conversion processes occurring. Lower numbers, on the other hand, indicate that the reactions happen more quickly. can be used to assess how disorderly the reactions are as they take place during the heat conversion process. Low values imply that the reaction system is likely to quickly reach its own thermodynamic equilibrium.

$$\Delta H = E_\alpha - RT \tag{7}$$

$$\Delta G = E_\alpha - RT_{peak}\ln\left(\frac{K_B T_{peak}}{hA}\right) \tag{8}$$

$$\Delta S = \frac{\Delta H - \Delta G}{T_{peak}} \tag{9}$$

Where T_{peak} is the peak temperature of DTG curve; K_B is the Boltzmann constant (1.381 × 10^{23}J/K); h is the Planck constant 6.626 × 10^{-34}J/s; heating rate (β)=15°C/min; R = 8.314 J/molK.

3. Results and discussion

3.1. Thermal analysis

TGA was used to assess the structural evolution and thermal degradation behavior of struvite crystals. In this case, different heat-transfer rates that influence the kinetics of thermal decomposition were investigated. The decomposition zone moved into the study's higher operating temperature, and the peak intensity increased as the heating rate increased, as shown in Fig 1(a) and (b). The thermal decomposition of struvite at various heating rates included simultaneous dehydration, decomposition, and liberation of H_2O and NH_3 molecules, as shown in Fig. 1. Otherwise, two distinct peaks would have been visible. The samples at various heating rates showed comparable trends in their weight loss profiles. Combustion is the first step, which ranges from about 0–100°C as shown by Fig 1(a) and (b), during this stage most bonds in the struvite crystals are likely to have fractured. The activation and decomposition is the second stage, from 150 to 300°C for all investigated heating rates and this is when significant mass loss was seen. The rate of degradation significantly decreased and was insignificant in the final stage from 250 to 350°C.

The theoretical mass loss for struvite is 51.42%, with water accounting for 44.08% and ammonia accounting for 7.34% (Wang et al., 2010). While using FCS as the magnesium source, the residual quantities for heating rates of 5°C/min;10°C/min and 15°C/min were lower than those of pure struvite at 47.9%, 47.4%, and 46.9% respectively. The literature indicated that the weight loss results were in good accord. The reduction in residue quantities demonstrated that the foreign ions in leached FCS co-precipitated with struvite forming other compounds with N and P.

The E_α is the absolute minimum amount of energy required to initiate a reaction; the lower the activation energy value, the more likely the reaction will occur. The average E_α for the conversion rates 0.3, 0,6 and 0.9 are shown in Table 1. As shown in Fig 2(a) to (d) the straight lines

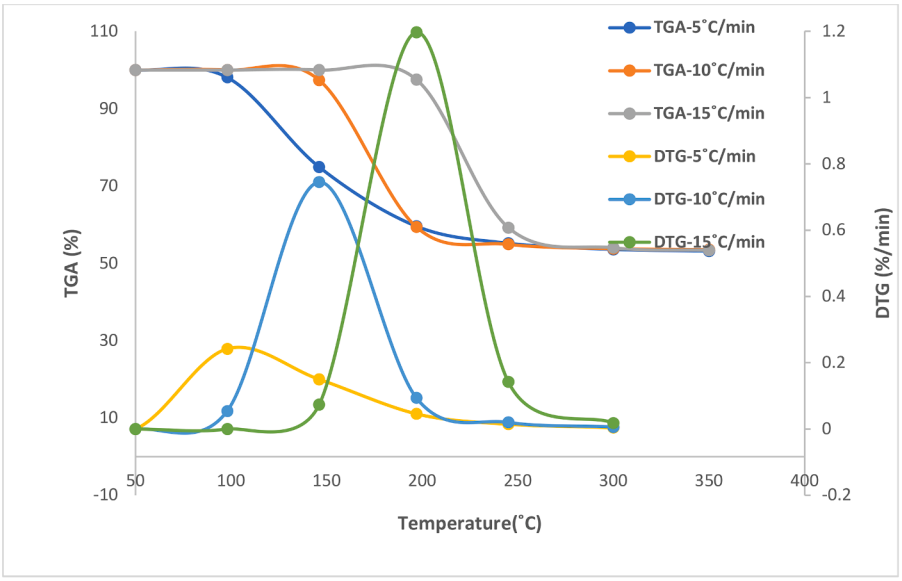

(a)

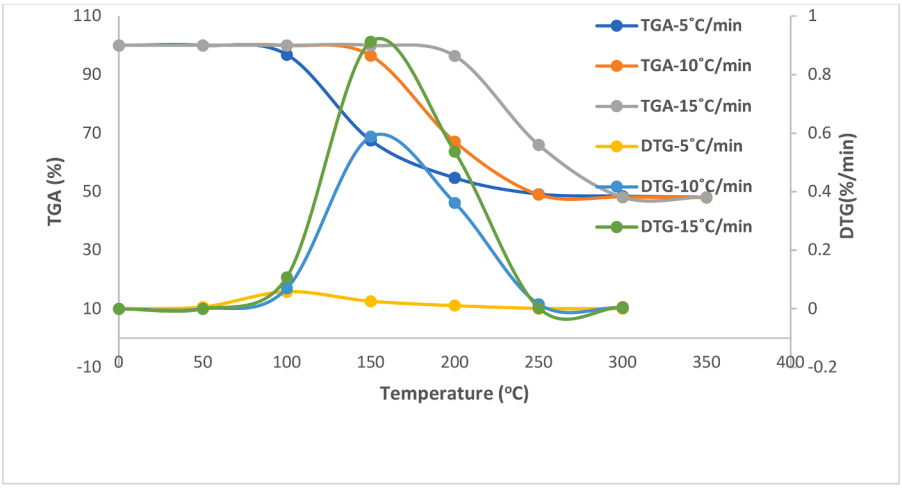

(b)

Fig. 1. Thermo-gravimetric analysis (TGA) curves at different heating rates obtained for struvite crystals prepared using (a) $MgCl_2$ (b) FCS.

Table 1
Activation energies and correlation coefficients from the model- free methods.

α	FWO E(kJ/mol)	R^2	KAS E(kJ/mol)	R^2	Starink E(kJ/mol)	R^2	Tang E(kJ/mol)	R^2
0.3	57.410	0.994	50.890	0.992	51.110	0.992	51.310	0.992
0.6	50.050	0.955	50.050	0.940	43.400	0.940	43.590	0.941
0.9	61.140	0.999	54.080	0.998	54.320	0.998	54.530	0.998
Average	***56.20***		***51.67***		***49.61***		***49.81***	

were obtained for the four models investigated. The straight-line parallelism of the plots reflected by the high R^2 (>0.9) values shown in table 1, indicate comparable kinetic activity and, most likely, the same reaction mechanism for struvite thermal degradation. Using the linear model equation, the E_α were calculated from the slopes (Mong et al., 2021). The E_α values for the models tested followed a similar pattern. They gradually decreased from a conversion of 0.3 to 0.6, then increased slightly from a conversion of 0.6 to 0.9. Table 1 shows that the FWO had the biggest difference in the average activation energy of 56.20 kJ/mol compared to KAS, Starink, and Tang models' which were 51.67, 49.61, and 49.81 kJ/mol, respectively. This implies that the FWO model is not appropriate in approximating activation methods. However, the values for the other aforementioned models were similar with the average value deduced by (Polat and Eral, 2022) of 49.2 kJ/mol

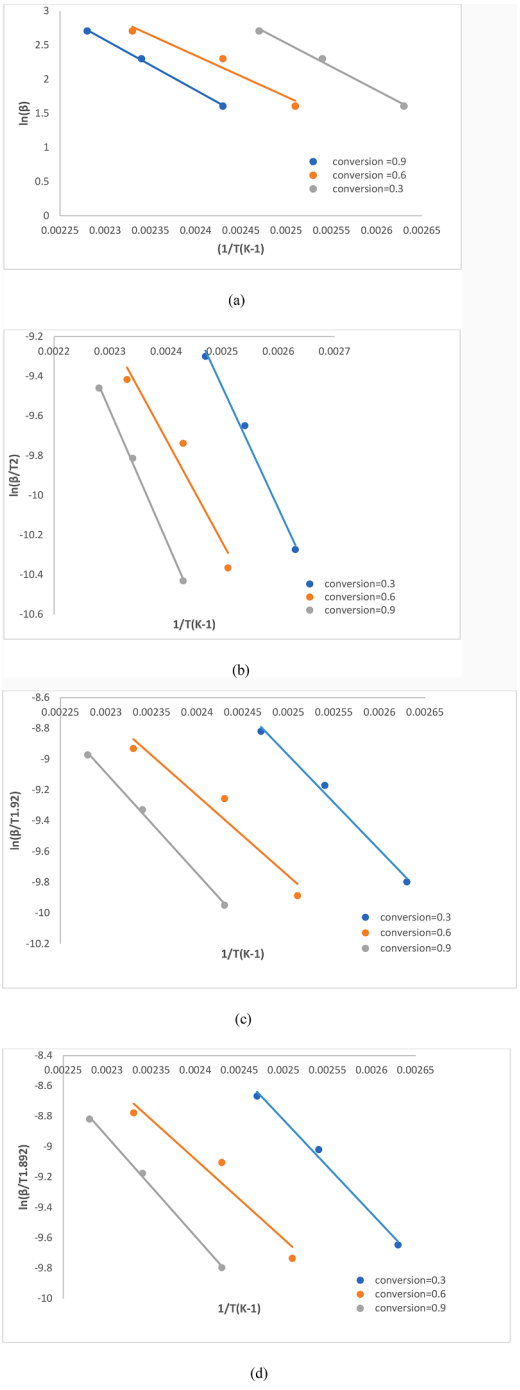

Fig. 2. Plots of (a) Flynn-Wall-Ozawa (b) Kissinger-Akahira-Sunose (c) Starink (d) Tang models of the struvite crystals using FCS at different heating rates.

using $MgCl_2$ as magnesium source for struvite precipitation from previous research. Since the calculated values are quite close, these activation energies, which were calculated using the four kinetic models and various heating rates, are consistent and reliable. The consistency and dependability of these activation energies, which were computed using the four kinetic models and different heating rates, is good across all models. The slight differences in activation energy values were caused by approximations, assumptions, and various mathematical formulations depending on the model.

A thorough examination of kinetics and thermodynamic parameters such as Gibbs free energy, enthalpy, and entropy change could provide detailed information regarding the nature of struvite crystal heat degradation. As a result, these parameters were computed, and the results as a function of temperature are presented in Table 2. Pre exponential factor (A) is an important kinetic parameter based on collision theory that is dictated by the reaction properties. A high value of $A \geq 1.67 \times 10^8 min^{-1}$ suggests that the reaction is multidimensional and complicated, whereas a value of $A \leq 1.67 \times 10^8 min^{-1}$ indicates that the reaction process is tied to the size of the surface area (Guan et al., 2023). Table 2 indicates that A values are less than $1.67 \times 10^8 min^{-1}$, showing that struvite crystal breakdown is a simple reaction. ΔH represents the energy difference before and after the chemical change of the struvite crystals which indicates the heat absorption and exothermic phenomena of the thermal degradation process (Guan et al., 2023). Heat is necessary to raise the energy level and change the struvite crystals to their transition states, as indicated by positive ΔH values. This suggests that the process is endothermic. The values of ΔG were deduced to be in the range of 127–147 kJ/mol, implying that the thermal breakdown of struvite crystals was not spontaneous. In theory, ΔS can provide information on system disorders during the thermal degradation process, and a negative number implies that the degree of disorder of the system is decreasing, and the system is approaching equilibrium.

To determine the ideal mechanism for struvite precipitation and the ideal reaction models for the process, the reaction models shown in Table 3 defined g(α). These reaction models have been proposed for kinetic analysis that takes diffusion, nucleation, and reaction into account (Polat and Sayan, 2020). The kinetic models used in this study are shown in Table 3. The Coats-Redfern method for kinetic analysis, which considers diffusion, reaction, or nucleation as rate limiting steps, proposed these reaction models (Polat and Sayan, 2020).

To accurately describe the kinetics of struvite precipitation, the plotting method was used. The greatest linearity represents the most likely reaction mechanism. Table 3 shows the kinetic models for the chemical reaction model, diffusion-controlled model, and nucleation model. Considering the correlation coefficient values (R^2) results in Table 4 it was observed that the chemical reaction model had the highest correlation for the struvite synthesized using FCS. The least correlation was observed in the diffusion-controlled model shown in Table 4 when using $MgCl_2$ as the magnesium source with R^2 values between 0.7 and 0.8. The crystallization reaction took place at 30°C, and previous research has shown that higher temperatures above 35°C usually result in diffusion-controlled growth, whereas lower temperatures result in surface integration-controlled growth (Li et al., 2013). Furthermore, stirring promotes struvite nucleation and thus increases crystal growth; thus, sufficient stirring is critical in this case, a constant stirring speed of 200 rpm was used to ensure that the crystallization process was not diffusion limited.

For all crystals, regardless of the media, Table 4 shows that the correlation coefficients generally reduced as the heating rate increased, implying that a lower heating rate was ideal. It was found that the second order reaction model was the best appropriate for defining the results after taking the correlation coefficient values into account.

3.2. Particle size

The median particle sizes of the final product after crystallization were measured and are shown in Fig 3. The analysis of particle size is critical for the design of the crystallization process, as well as the

Table 2
Thermodynamic and kinetic parameters for thermal degradation of struvite crystals.

Conversion	A (min^{-1})	ΔH(kJ/mol)	ΔG (kJ/mol)	ΔS (kJ/mol)
0.3	1.88×10^6	47.579	143.736	−0.205
0.6	4.53×10^5	50.177	146.929	−0.206
0.9	2.21×10^5	39.260	127.949	−0.189
Average	**2.21×10^6**	**45.672**	**139.538**	**−0.200**

Table 3
Different kinetic models chosen for the study (Polat and Sayan, 2020; Burns et al., 2021).

Model No.	Reaction mechanism	g(α)
Diffusion controlled models		
1.	One dimensional diffusion	α^2
2.	Two-dimensional diffusion (Valensi equation)	$\alpha + [(1-\alpha)\ln(1-\alpha)]$
3.	Three-dimensional diffusion (Jander equation)	$[[1-(1-\alpha)^{1/3}]^2$
4.	Anti-Jander equation	$[1+\alpha)^{1/3}-1]^2$
5.	Three-dimensional diffusion (Ginstling-Brounstein equation)	$1-(2/3)\alpha-(1-\alpha)^{2/3}$
Nucleation reaction models		
6.	Power law	α
7.	Power law	$\alpha^{1/2}$
8.	Power law	$\alpha^{1/3}$
9–11 $n = 2,3,4$ (Avrami-Erofeev)		$[-\ln(1-\alpha)]^{1/n}$
Chemical reaction models		
12.	First order (Mampel)	$(-\ln(1-\alpha))$
13.	Reaction order $n = 2$	$[(1-\alpha)^{1-n}-1]/n-1$
Phase boundary reaction models		
14.	Contraction of cylinder	$1-(1-\alpha)^{1/2}$
15.	Contraction of sphere	$1-(1-\alpha)^{1/3}$

Table 4
Correlation coefficients for the struvite prepared using $MgCl_2$ and FCS.

Model No.	Correlation coefficients (R^2)					
	$MgCl_2$			FCS		
	5°C/min	10°C/min	15°C/min	5°C/min	10°C/min	15°C/min
Diffusion controlled models						
1	0.900	0.833	0.829	0.901	0.826	0.826
2	0.903	0.756	0.749	0.892	0.815	0.810
3	0.870	0.795	0.781	0.844	0.843	0.824
4	0.891	0.839	0.835	0.897	0.818	0.817
5	0.923	0.817	0.796	0.919	0.873	0.873
Nucleation reaction models						
6	0.869	0.856	0.851	0.880	0.815	0.814
7	0.869	0.856	0.851	0.880	0.815	0.814
8	0.816	0.874	0.871	0.833	0.847	0.846
9	0.982	0.915	0.867	0.985	0.917	0.901
10	0.938	0.951	0.918	0.967	0.927	0.912
11	0.921	0.956	0.934	0.935	0.926	0.912
Chemical reaction models						
12	0.888	0.895	0.796	0.874	0.953	0.940
13	0.603	0.497	0.473	0.658	0.667	0.852
Phase boundary reaction models						
14	0.928	0.812	0.798	0.925	0.823	0.816
15	0.975	0.926	0.879	0.969	0.927	0.903

operation of struvite crystallizers (settleability) and post-handling steps such as filtration and drying (Shaddel et al., 2020). Fig. 3 shows that the median particle size and crystal formation rate were both larger at pH values of 7.5 and 8. This can be attributed to aspects such as co-precipitation, surface adsorption, the incorporation of extra anions or cations into the lattice of a growing crystal as part of a stable solid solution or through entrapment, and even the actual physical inclusion of mother liquor pockets. Foreign ions are present in FCS, consequently other compounds besides struvite can co-precipitate at a lower pH (Kabdasli et al., 2017). Whilst at high solution pH, it was found that small aggregate sizes predominated (Ye et al., 2014).

The competition between the nucleation and crystal growth rates, the two fundamental stages of crystallization, affects the crystal size distribution, which is a typical key indicator of product quality. Small crystals are frequently the result of quick nucleation and sluggish development, whereas large crystals frequently result from slow nucleation and rapid growth (Mehta et al., 2013). The beginning of nucleation brought on by high super saturation from the one-time injection of NaOH is what causes the development of tiny particles. During crystallization, particles may expand individually or in groups. Larger aggregates settle faster and make granulation in the reactor easier, making struvite crystal aggregation desirable for wastewater applications. The increased structural strength of struvite pellets is reportedly due to the clustering of small struvite crystals.

In general, phosphorus elimination is more effective at pH 9 than at pH 7.5, with an efficiency of above 90% (Li et al., 2019). A substantial percentage of tiny particles are present at pH 9 and 9.5, a negligible number at pH 7.5, and a relatively smaller percentage at pH 8 and 8.5, as shown in Fig. 4. The pH of the solution unexpectedly rose above 7 when all the NaOH was added at once. Due to the quick dynamics of the process, this causes a nucleation burst that consumes virtually all the super saturation, leaving little room for the growth phase, which produces a lot of small particles (Guan et al., 2023). Fig. 4 further demonstrates that using $MgCl_2$ at Mg:P ratio of 1 results in a large amount of fines at a pH of 9. As opposed to when FCS solution is used, which contains ferric chloride and is successful in reducing suspended material, in this case, suspended material may be present due to inadequate coagulation. Since this suspended material is primarily made up of organic stuff, it is naturally negatively charged. Electrostatic repulsion is the result, and repulsion between the organic material and the initially formed struvite. This impedes the agglomeration process resulting in finer particles. This suspended material can also block the active growth sites for struvite crystallization resulting in finer particles. Moreover, the number of nucleation sites increases at the presence of suspended material resulting in heterogeneous nucleation which will compete with crystal growth ensuring formation of more fine particles (Desmidt et al., 2013). Chemical dosage also increases a solution's ionic strength, which may increase the dissolution potential of struvite, resulting in larger particles being reduced to finer particles at higher pH levels.

The crystal development of struvite is constrained by its zeta potential, according to earlier studies. The negative zeta potential of struvite crystals prevents agglomeration, which promotes the growth of tiny particles. Considering Fig. 4, as the pH rises, the zeta potential and electrostatic repulsion increase, preventing the formation of crystals and producing finer particles. Additionally, the reaction occurred at room temperature, which is a low temperature because it is less than 30 °C. Low temperatures promote the growth of tiny particle sizes because they inhibit crystal nucleation and growth. As a result, limiting operational conditions to low P concentrations and mild alkaline pH would produce compact structures, large aggregate sizes, and high aggregation strength (Ye et al., 2014). The size of particles can be improved by inducing collision of particles and allowing for a sufficient period for particles to adhere together.

3.3. Surface morphology

Fig 5 shows that the surface of the precipitate was smooth when $MgCl_2$ was added, but it had a few tiny crystals on it after ferrochrome slag was added. On the surface of the precipitate that had FCS added to it, there were also several small crystals. This observation has also been reported in several reports. Numerous crystal morphologies (such as prismatic, pyramidal, coffin-shaped, feather-like, and needle-shaped) can exist depending on the growth conditions, according to studies on the formation of struvite. Hydrogen bonds hold the distorted PO_4^{3-} octahedrons of $Mg(H_2O)_6^{2+}$ and an octahedron group of NH_4^+ together to create the orthorhombic crystals that make up pure struvite.

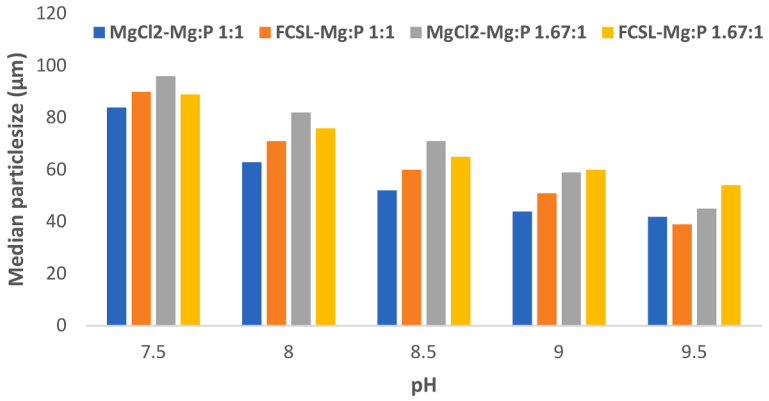

Fig. 3. Median particle size for Ferrochrome slag (FCS) and $MgCl_2$.

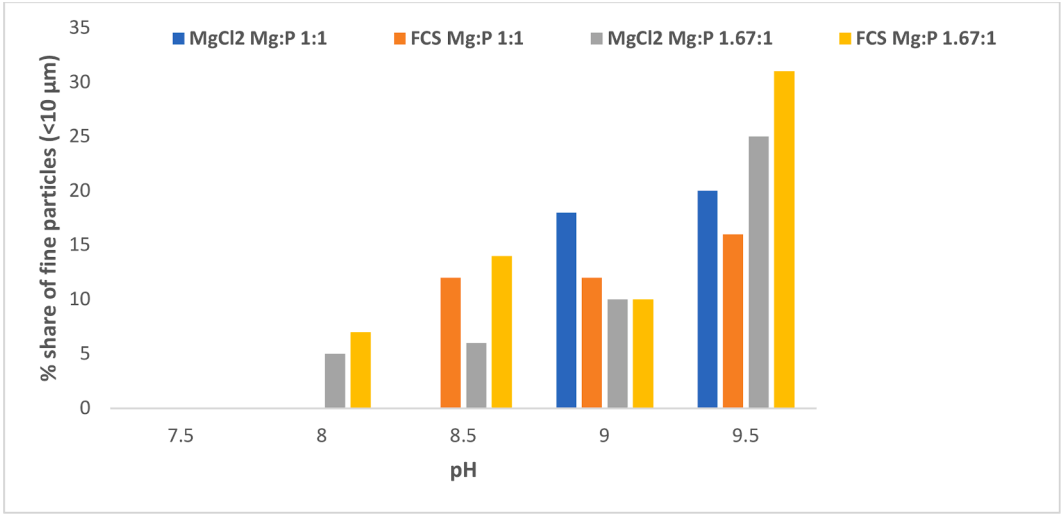

Fig. 4. Share of fine particle sizes for struvite produced using FCS and $MgCl_2$.

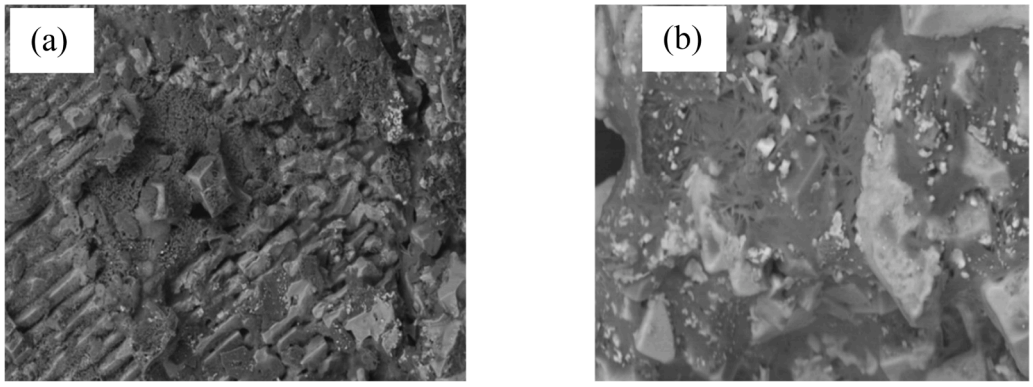

Fig. 5. Surface morphology for struvite crystals synthesized using FCS at pH 9.5, Mg:N:P ratio1 1.2:1:1.15: (a) at 100 µm magnification, (b) at 20 µm magnification.

Fig 5(a) and (b) shows that when these conditions of excess super saturation exist, the struvite morphology may shift from needle to dendritic geometries, with X-shaped as an intermediate stage. Pure struvite was identified by the X-shaped dendritic envelope and rectangular-like structures. Fig. 5 depicts particles with an X-shaped morphology (b), this could be interpreted as a stage in the transition from well-faceted to dendritic crystals, or it could be interpreted as an inferred boundary between slow and rapid growth. The X-shaped crystals are created by combining a variety of unique crystals. Previous studies have suggested that the crystals' development orientations are influenced by the interior structure of the struvite. Struvite, which produces surfaces with a higher potential and chance of growing directions, regulates the final shape of struvite crystals. A tabular form is recommended from the perspective of process engineering because of its more uniform shape and lower tendency to break into smaller fragments (Mehta and Batstone, 2013). Fig. 5(a) and (b) also show the presence of fines. This may be attributed to that nucleation took place at a pH of 9.5, which was attained by adding NaOH only once. This one-time addition

of NaOH causes the pH to rise sharply above the metastable zone resulting in rapid formation of fines. Moreover, the precipitation of counter ions like Zn, Cu, and Ca in solution causes co-precipitation of isolated fine particles which in this case will include to form hydroxides, oxides, and other particles due to the limiting concentrations.

4. Conclusion

This study demonstrated the characteristics of the struvite that forms when FCS is used as a substitute for magnesium. The particle size distribution of struvite crystals was significantly affected as it decreased from a maximum median size of 96 μm to a minimum median size of 35 μm as pH increased from 7.5 to 9.5. The highest percent of fines (<10 μm) was recorded at a pH of 9.5 using FCS as magnesium source in the metastable region of struvite precipitation whereas at a pH of 7.5 no fines (<10 μm) were recorded. This indicated that a lower pH is ideal for formation of large particles. Chemical reaction model kinetics provided the best description of the reported crystallization process, with a positive and high R^2 value indicating good linearity. Model fitting was used to determine the reaction control mechanism and the average activation energies obtained by four model free methods were FWO (56.2), KAS (51.67) Starink (49.61) and Tang (49.81) kJ/mol. The thermodynamic data indicated that the thermal degradation of struvite crystals has a high degree of disorder, and the process is endothermic, irreversible and non-spontaneous. The surface morphology of the finished product indicated presence of various shape variations and the presence of tiny particles clumping together with larger crystals. Along with managing the factors that influence the crystallization process, seeding which entails incorporating preformed struvite crystals before the precipitation is advised to prevent the formation of a significant amount of fine particles and ensure that the crystals that do form are of a more uniform compact size and shape.

Declaration of competing interest

The authors whose names are listed immediately below certify that they have NO affiliations with or involvement in any organization or entity with any financial interest (such as honoraria; educational grants; participation in speakers' bureaus; membership, employment, consultancies, stock ownership, or other equity interest; and expert testimony or patent-licensing arrangements), or non-financial interest (such as personal or professional relationships, affiliations, knowledge or beliefs) in the subject matter or materials discussed in this manuscript.

References

Burns, M., Sheehan, M., Schneider, P.A., 2021. Nucleation and crystal growth kinetic parameter optimization of a continuous poiseuille flow struvite crystallizer using a discretized population balance and dynamic fluid model. Chem. Eng. J. 405, 126607.

CNBC, 2022. A Fertilizer Shortage, Worsened by War in Ukraine, is Driving up Global Food Prices and Scarcity. CNBC. Available at. https://www.cnbc.com/2022/04/06/a-fertilizer-shortage-worsened-by-war-in-ukraine-is-driving-up-global-food-prices-and-scarcity.html. Accessed: 20 August 2023.

Das, S.K., Tripathi, A.K., Kandi, S.K., Mustakim, S.M., Bhoi, B., Rajput, P., 2023a. Ferrochrome slag: a critical review of its properties, environmental issues and sustainable utilization. J. Environ. Manage. 326, 116674 https://doi.org/10.1016/j.jenvman.2022.116674.

Fao.org (2022) *Zimbabwe at a glance | FAO in Zimbabwe | Food and Agriculture Organization of the United Nations*. Available at: https://www.fao.org/zimbabwe/fao-in-zimbabwe/zimbabwe-at-a-glance/en/(Accessed: 20 August 2023).

Desmidt, E., Ghyselbrecht, K., Monballiu, A., Rabaey, K., Verstraete, W., Meesschaert, B. D., 2013. Factors influencing urease driven struvite precipitation. Sep. Purif. Technol. 110, 150–157. https://doi.org/10.1016/j.seppur.2013.03.010.

Guan, W., Han, Z., Su, W., Guo, S., Guo, Y., 2023. Comprehensive study of thermal deradation behavior of carbon fiber flexible sucker rods: product characteristics, kinetics and thermodynamics. Fuel 333, 126306.

Kabdaşlı, I., Atalay, Z., Tünay, O., 2017. Effect of solution composition on Struvite crystallization. J. Chem. Technol. Biotechnol. 92 (12), 2921–2928.

Li, J., Song, C., Su, Y., Long, H., Huang, T., Yeabah, T.O., Wu, W., 2013. A study on influential factors of high-phosphorus wastewater treated by electrocoagulation–ultrasound. Environ. Sci. Pollut. Res. 20 (8), 5397–5404.

Mehta, C.M., Batstone, D.J., 2013. Nucleation and growth kinetics of struvite crystallization. Water Res. 47 (8), 2890–2900.

Moyo, L.B., Simate, G.S., Mamvura, T.A., 2022a. Magnesium recovery from ferrochrome slag: kinetics and possible use in a circular economy. Heliyon 8 (12).

Moyo, L.B., Simate, G.S., Mutsatsa, T., 2022b. Biological acidification of pig manure using banana peel waste to improve the dissolution of particulate phosphorus: a critical step for maximum phosphorus recovery as struvite. Heliyon 8 (8).

Moyo, L.B., Simate, G.S., Mamvura, T.A., Danha, G., 2023. Recovering phosphorus as struvite from anaerobic digestate of pig manure with ferrochrome slag as a magnesium source. Heliyon 9 (4).

Muryanto, S., Bayuseno, A.P., 2014. Influence of Cu^{2+} and Zn^{2+} as additives on crystallization kinetics and morphology of struvite. Powder Technol. 253, 602–607.

Ping, Q., Li, Y., Wu, X., Yang, L., Wang, L., 2016. Characterization of morphology and component of struvite pellets crystallized from sludge dewatering liquor: effects of total suspended solid and phosphate concentrations. J. Hazard. Mater. 310, 261–269.

Polat, S., Eral, H.B., 2022. Effect of hyaluronic acid on the struvite crystallization: a structural, morphological, and thermal analysis study. J. Cryst. Growth 592, 126734. https://doi.org/10.1016/j.jcrysgro.2022.126734.

Polat, S., Sayan, P., 2020. Preparation, characterization and kinetic evaluation of struvite in various carboxylic acids. J. Cryst. Growth 531, 125339. https://doi.org/10.1016/j.jcrysgro.2019.125339.

Santiviago, C., Peralta, J., López, I., 2022. Phosphorus removal from wastewater through struvite crystallization in a continuous fluidized-bed reactor: an improved comprehensive model. Chem. Eng. J. 430, 132903.

Shaddel, S., Grini, T., Andreassen, J.P., Østerhus, S.W., Ucar, S., 2020. Crystallization kinetics and growth of struvite crystals by seawater versus magnesium chloride as magnesium source: towards enhancing sustainability and economics of Struvite crystallization. Chemosphere 256, 126968.

Song, L., Li, Z., Wang, G., Tian, Y., Yang, C., 2021. Supersaturation control of Struvite growth by operating ph. J. Mol. Liq. 336, 116293.

Wang, C.C., Hao, X.D., Guo, G.S., van Loosdrecht, M.C.M., 2010. Formation of pure struvite at neutral ph by electrochemical deposition. Chem. Eng. J. 159 (1–3), 280–283. https://doi.org/10.1016/j.cej.2010.02.026.

Wu, J., Li, Y., Xu, B., Li, M., Wang, J., Shao, Y., Chen, F., Sun, M., Liu, B., 2022. Effects of physicochemical parameters on struvite crystallization based on kinetics. Int. J. Environ. Res. Public Health 19 (12), 7204.

Ye, Z., Shen, Y., Ye, X., Zhang, Z., Chen, S., Shi, J., 2014. Phosphorus recovery from wastewater by struvite crystallization: property of aggregates. J. Environ. Sci. 26 (5), 991–1000.

Zhang, T., Jiang, R., Deng, Y., 2017. Phosphorus recovery by struvite crystallization from livestock wastewater and reuse as fertilizer: a Review. Physico-Chem. Wastewater Treat. Resour. Recov. https://doi.org/10.5772/65692.